# Dopant location identification in $Nd^{3+}$-doped $TiO_2$ nanoparticles

W. Li
*Department of Materials Science and Engineering, University of Delaware, Newark, Delaware 19716, USA*

A. I. Frenkel
*Department of Physics, Yeshiva University, New York, New York 10016, USA*

J. C. Woicik
*National Institute of Standards and Technology, Gaithersburg, Maryland 20899, USA*

C. Ni
*Department of Materials Science and Engineering, University of Delaware, Newark, Delaware 19716, USA*

S. Ismat Shah*
*Department of Physics and Astronomy, University of Delaware, Newark, Delaware 19716, USA*
*and Department of Materials Science and Engineering, University of Delaware, Newark, Delaware 19716, USA*
(Received 8 March 2005; revised manuscript received 12 August 2005; published 19 October 2005)

Large band gap semiconductors are typically doped in order to enhance their photocatalytic, photovoltaic, and other chemical and optoelectronic properties. The identification of dopant position and its local environment are essential to explore the effect of doping. X ray techniques, including extended x ray absorption fine structure, x ray photoelectron spectroscopy, and x ray diffraction, were performed to analyze the Nd (0 to 1.5 at. %) dopant location and the structural changes associated with the doping in anatase $TiO_2$ nanoparticles, which were synthesized by metalorganic chemical vapor deposition. Nd ions were determined to have a trivalent chemical state and substitute for $Ti^{4+}$ in the $TiO_2$ structure. The substitutional $Nd^{3+}$ ions cause anatase lattice expansion along *c* direction with a maximum value of 0.15 Å at 1.5 % Nd doping level and the local structure of the dopants changes towards rutile like configuration. The lengths of the nearest neighbor Nd-O and Nd-Ti bonds increase by 0.5–0.8 Å compared to their counterparts in the pure $TiO_2$ host structure. The substitutional nature of $Nd^{3+}$ dopants explains why they are efficient not only for charge carrier separation but also for visible light absorption in $TiO_2$.

DOI: 10.1103/PhysRevB.72.155315 PACS number(s): 61.10.Ht, 61.46.+w, 61.72.−y

## I. INTRODUCTION

Doping methods have been extensively utilized for modifying the electronic structures of $TiO_2$ nanoparticles to achieve new or improved catalytic,[1] electroptical,[2,3] magnetic,[4] and other chemical and physical properties. Dopants can segregate on $TiO_2$ nanostructure surfaces or they can be incorporated into the lattice, where the dopants can be on substitutional, interstitial or both sites. Dopants with different locations have different impact on the $TiO_2$ properties. For instance, the effect of dopants on $TiO_2$ photoreactivity critically depends on dopant location and coordination in the particles. It is mostly the substitutional dopant ions that contribute to the change of electronic structure and light absorption efficiency of the host. The substituational dopant ions can induce an electronic coupling effect with the host atoms and bring possible electron states within the band gap of the semiconductors. The dopant related localized states on either the top of the valence band or below the conduction band are favorable to the band gap change, which in turn affects the photon absorption. For example, the anatase $Ti_{1-x}N_xO_2$ has been confirmed to be active to the visible light rather than only ultraviolet due to the presence of well localized N 2p on the top of O 2p valence band.[5]

The location and the local bonding configurations of the dopants in $TiO_2$ are difficult to predict theoretically. The coordination environment of the dopants is affected not only by the nature of the dopant such as ionic radii and concentration but also by the synthesis method. For dopant ions with sizes comparable to that of the host ions, it is conceivable that it would be easier for them to occupy the host sites as opposed to the dopants that have much larger or much smaller radii. Thermodynamically, the quantity of dopants in the lattice will be limited by the maximum equilibrium solid solubility limit of the dopants in $TiO_2$ nanoparticles. For different synthesis processes, the dopant position may also change. Dopant ions are initially absorbed on the surface of $TiO_2$ particles during the hydrolysis step in the sol-gel method. A part of these ions are then incorporated in substitutional or interstitial sites of $TiO_2$ after calcination.[6] The dopant may also form separate dopant related phase(s) during the calcination process, such as the formation of the $CoTiO_3$ phase in the $Co^{3+}$ doped $TiO_2$ by sol-gel.[7] In spite of a large quantity of literature dealing with the effect of dopants on the chemical and physical properties of $TiO_2$, there is very little information available on the location of the dopant and their local environment. The lack of a complete description of the dopant locations in the host is one of the sources which resulted in many contradictory properties for the same type of dopants even when the concentration levels of the dopants were the same. For example, there is disagreement about whether the $Cr^{3+}$ dopant enhances or inhibits the photoactivity of

 

$TiO_2$.[8–11] A similar controversy also exists for $Fe^{3+}$ doped $TiO_2$.[12–14] Therefore, to better understand the role of the dopants, it is important to use appropriate characterization techniques to measure the local structures of the dopants in a $TiO_2$ lattice. Such information will also help with the selection of the right dopant for the specific application of $TiO_2$ nanoparticles.

Extended x ray absorption fine structure (EXAFS) is a powerful technique due to its direct measurement of short-range structural details selectively, i.e., around x ray absorbing atoms in the sample. It has been successfully applied to obtain local environment information of dopants.[15–20] In this paper, the dopant Nd location and its local structure in $TiO_2$ nanoparticles synthesized by metalorganic chemical vapor deposition (MOCVD) have been determined. Structural distortions of $TiO_2$ at various concentrations, 0 to 1.5 at. %, of $Nd^{3+}$ are investigated by using EXAFS and other x ray techniques. Expansion of the unit cell and changes in the local structure around dopants are observed in the doped samples. In the previous study, we have reported Nd induced tailoring of $TiO_2$ band gap.[21] This work obtains the structural model of $Nd^{3+}$ ion doping, namely, that $Nd^{3+}$ ions enter the $TiO_2$ lattice substitutionally. Such a mechanism of doping allows the possibility to introduce electron states into the band gap.

## II. EXPERIMENT AND DATA ANALYSIS

All Nd doped and undoped $TiO_2$ nanoparticles were synthesized by MOCVD. The details of the deposition system and sample preparations were described elsewhere.[21,22] The particle size and crystal structures were respectively determined by dark field images and selected area diffraction patterns obtained from transmission electron microscopy (TEM). The crystal structures and average size were confirmed and the crystal lattice constants were determined by x ray powder diffraction (XRD), which is equipped with a graphite crystal monochromator using Cu $K_\alpha$ radiation ($K_{\alpha 1}=1.5405$ Å and $K_{\alpha 2}=1.5444$ Å). Besides the range scans ($2\theta=20°-60°$), high resolution scans for anatase (101) and (200) peaks were carried out with scan speed of 0.05° min and short point interval of 0.002°. To precisely determine the peak positions, the $K_{\alpha 1}$ and $K_{\alpha 2}$ peaks were resolved. The lattice constants were calculated based on (101) and (200) peak positions. The surface composition and dopant state of the samples were determined by x ray photoelectron spectroscopy (XPS), which employs Al $K_\alpha$ exciting radiation as x ray source. High resolutions scans were done for Nd (4d) peaks to verify the dopant chemical state. The chemical compositions were also analyzed by energy dispersive x ray spectroscopy (EDS), which is attached to a scanning electron microscopy system.

Local structure change of the dopant Nd in the $TiO_2$ was investigated by using EXAFS. Nd $L_3$-edge and Ti K-edge EXAFS data were collected at the UNICAT beamline facility 33 BM at the Advanced Photon Source and at the NIST beamline facility X23-A2 at the National Synchrotron Light Source. The Nd data from the Nd doped $TiO_2$ were measured by collecting the Nd fluorescence using a large area ionization chamber. The transmission mode was used to measure the $Nd_2O_3$ and $TiO_2$ standards.

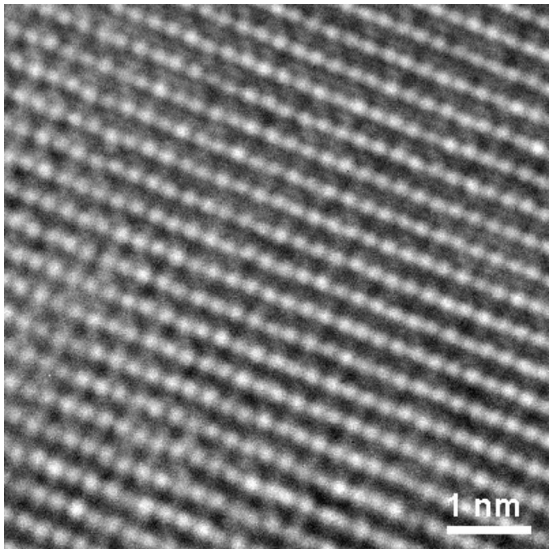


FIG. 1. A high resolution TEM atomic image of 1.5 % Nd doped $TiO_2$ nanoparticles.

## III. RESULTS AND DISCUSSION

### A. Structural and chemical analysis

All $TiO_2$ nanoparticle samples in this experiment have anatase crystal structure with an average size around 22 nm. The anatase crystal structure was confirmed by the selected area electron diffraction patterns analysis. The diffraction patterns showed typical anatase diffraction rings from crystal planes including (101), (004), (200), and (105). The anatase structure and average size of the samples is also consistent with the XRD measurements. The analysis of the structure and particle size by TEM and XRD has already been reported elsewhere.[21] Figure 1 is a high resolution transmission electron microscopy lattice image of 1.5 at. % Nd doped anatase $TiO_2$ nanoparticles. However, at such a low level of doping, no specific dopant related regions could be identified in this lattice image.

Dopant concentrations and chemical states were obtained from EDS and XPS, respectively. The Nd concentrations range from 0 to 1.5 at. % and the corresponding ratios of Nd:Ti extended from 0 to 0.046.[21] Figure 2 shows the high resolution XPS scans of Nd 4d region of the doped samples. All the Nd 4d peaks are positioned at around 122 eV, which are shifted from a metallic $Nd^0$ peak position (118 eV).[23] The positive binding energy shift of Nd 4d results from the decrease of electron density, suggesting that the dopant is present as $Nd^{3+}$ ions in the $TiO_2$ nanoparticles.[24,25] The quantification of the chemical state is helpful for further exploring the detailed $Nd^{3+}$ associated chemical bonding information in the crystal lattice, such as bond lengths.

### B. Average lattice distortion

XRD shows a lattice constant change upon doping $TiO_2$ with Nd. No separate dopant related phases were found suggesting little or no dopant oxide phase within the XRD detection limit. However, both (101) and (200) peak positions

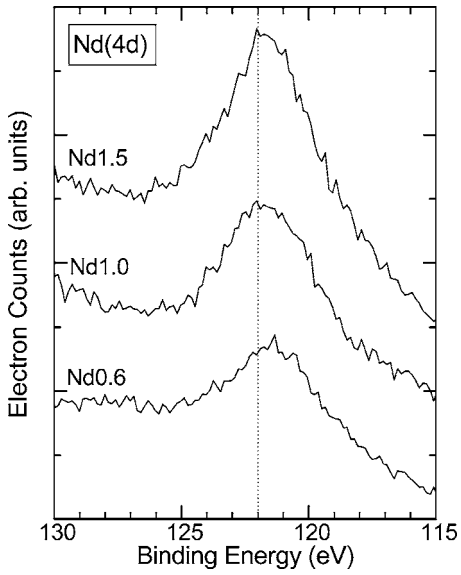


FIG. 2. XPS of Nd 4d region for samples with various Nd doping concentrations.

showed a slight shift to the smaller angles with the increase of Nd concentration. Figure 3(a) shows the XRD patterns for (101) peaks of doped and undoped samples. Peak fits for the $K\alpha_1$ (solid line), $K\alpha_2$ (dotted line), and the composite fit are shown. The figure shows that the lattice space is enlarged after the doping. The $TiO_2$ lattice constants were calculated based on anatase (101) and (200) diffraction peak positions and the characteristics of anatase tetragonal structure. Figure 3(b) plots the lattice constants "a" and "c" as a function of Nd concentration. The lattice constant increase is observed with the increase of Nd level along the *c*-axis only. The lattice constant "a" along the basal planes remains more or less constant. The maximum elongation of *c*-axis is about 0.15 Å, from 9.516 Å (0% Nd) to 9.671 Å (1.5% Nd). The lattice expansion from XRD indicates the possibility of $Nd^{3+}$ ions substituting $Ti^{4+}$ sites because of the large difference of the ionic radii between the dopant and host ions ($Nd^{3+}$:0.983 Å and $Ti^{4+}$:0.605 Å, with a coordination number of 6[26]) causing the enlargement of the $TiO_2$ lattice constant. Nevertheless, XRD determines only the average periodic structure and does not offer insights to any local structural distortion.

### C. Local structure around dopants

In this section we present analysis and results for the first and second nearest neighbor shells of Nd obtained by EXAFS. EXAFS data were analyzed by an IFEFFIT[27] package. For each measured X ray absorption spectrum, the AUTOBK code[28] was used to normalize the absorption coefficient, $\mu(k)$, by the absorption edge step and separate the EXAFS, $\chi(k)$, from the isolated atom absorption background, $\mu_0(k)$:

$$\chi(k) = \frac{\mu(k) - \mu_0(k)}{\Delta\mu_0(k)},$$

where $k$ is the photoelectron wave number, $k = \sqrt{2m(E-E_0)/\hbar^2}$, $E$ is the photon energy, and $E_0$ is the photoelectron energy origin (chosen at the middle of the absorption edge jump). Figure 4 shows the $k^2$-weighted EXAFS for the $Nd_2O_3$ reference and two doped samples. Visual examination of the data shows that the local environment in the doped samples, while similar for the 1 % and 1.5 % dopings, is drastically different from that in the $Nd_2O_3$ structure. These data are, therefore, inconsistent with any model that assumes Nd atoms segregating into $Nd_2O_3$-rich local regions in a $TiO_2$ host.

Figure 5(a) depicts the Fourier transform magnitudes of Ti K-edge $k^2$-weighted $\chi(k)$ data and fit of the data for pure rutile $TiO_2$. This sample was analyzed first, in order to calibrate our modeling strategy against the known structure of a model compound, which is also a prototype local structure of Nd entering rutile $TiO_2$ structure substitutionally. The data *k*-range was 2–10.5 $Å^{-1}$. Fitting was performed by a nonlinear least square method employed in IFEFFIT that utilizes theoretical scattering amplitudes and phases of the photoelectron calculated by FEFF6 code.[29] Fitting was performed within the *r*-range (1.1–3.4 Å) corresponding to the following *n*-degenerate shells of Ti nearest-neighbor linkages (only single-scattering photoelectron paths were obtained to dominate EXAFS in this range): $n=6$ for Ti-O1, 2 for Ti-Ti2, and 8 for Ti-Ti3 pairs in rutile $TiO_2$ structure [Figure 6(a)].[30,31] As described below, we did not include the Ti-O2 pairs (Table I) for pure $TiO_2$ since they contribute in the same distance range as Ti-Ti2, the latter being much stronger contribution as obtained by FEFF simulation. We varied six variables: the $\Delta E_0$ correction to the photoelectron energy origin, the isotropic lattice expansion/contraction factor, the ampli-

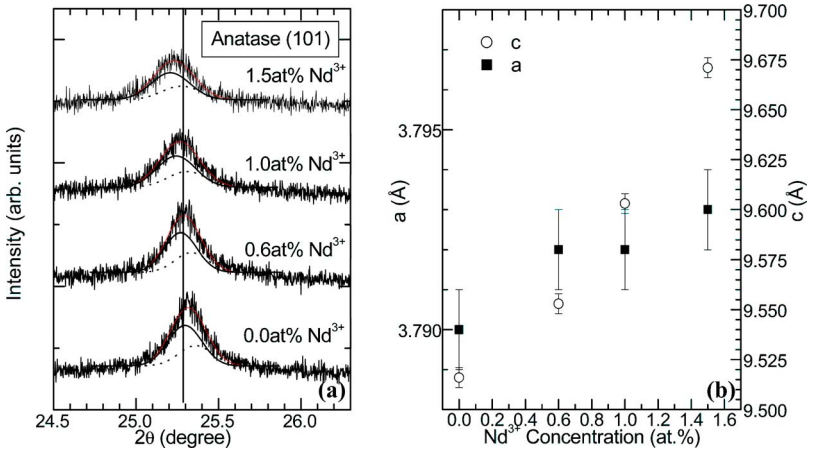


FIG. 3. (Color online) (a) XRD anatase (101) diffraction peaks; (b) $TiO_2$ lattice parameters "a" and "c" (right) as a function of Nd concentration.

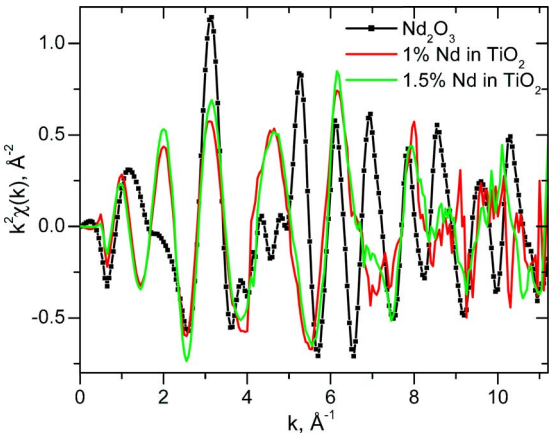


FIG. 4. (Color online) $k^2$-weighted, background subtracted and edge-step normalized Nd $L_3$-edge EXAFS data in the reference $Nd_2O_3$ and two doped samples.

tude reduction factor, and three Debye-Waller factors, for each shell independently. Nearest neighbor distances obtained in the fit (Table I) were found within the error bars from the tabulated crystallographic values, thus attesting our fitting procedure as reliable.

Similar analysis procedure was applied to fit the Nd $L_3$-edge EXAFS spectra of $Nd_2O_3$ and Nd:$TiO_2$ samples. The spectra of 1 % Nd doped $TiO_2$ and the $Nd_2O_3$ reference are shown in Figs. 5(b) and 5(c), respectively. Figure 5(b) presents the best fit of the Nd:$TiO_2$ EXAFS assuming that Nd substitutes for Ti in rutile $TiO_2$. Theoretical FEFF paths Nd-O1, Nd-Ti1, Nd-Ti2, and Nd-O2 were calculated and the theoretical EXAFS signal was then fit to the data in *r*-space by varying corrections to the model distances of these pairs, the Debye-Waller factors, and the $\Delta E_0$ correction. The amplitude reduction factor was not varied in the fits and held equal to its value obtained from the analysis of the $Nd_2O_3$ reference compound. Best fit results for the Nd nearest neighbor pair distances are tabulated in Table I for both doped samples. Interestingly, while separate refining of Ti-O2 and Ti-Ti2 contributions to the Ti K-edge EXAFS in $TiO_2$ is hindered due to the interference of these pairs contribution to EXAFS; such degeneracy can be lifted if the lengths are no longer similar. In the case of Nd:$TiO_2$, both types of paths can be resolved by EXAFS.

The local structure of Nd in the $Nd_2O_3$ reference compound was also fit by using the most dominating single-scattering photoelectron paths calculated theoretically by FEFF6 for the Nd-O and Nd-Nd bonds by using available crystallographic information.[32] The crystal structure of this compound contains 8 Nd-O and 12 Nd-Nd pairs in the nearest-neighboring shells, and its EXAFS is drastically different from those in the Nd:$TiO_2$ samples (Figs. 4 and 5).

It is important to emphasize that we also attempted to fit the local structure of Nd in the Nd:$TiO_2$ samples to other models including Nd with anatase local structure, Nd with $Nd_2O_3$ local structure, and Nd with $Nd_2O_3$ local structure with Ti replacing Nd in the second (metal) shell. Interestingly, the best fit quality was obtained for the model where the local structure around Nd is the same as that around Ti in rutile $TiO_2$. These results are discussed in the following section.

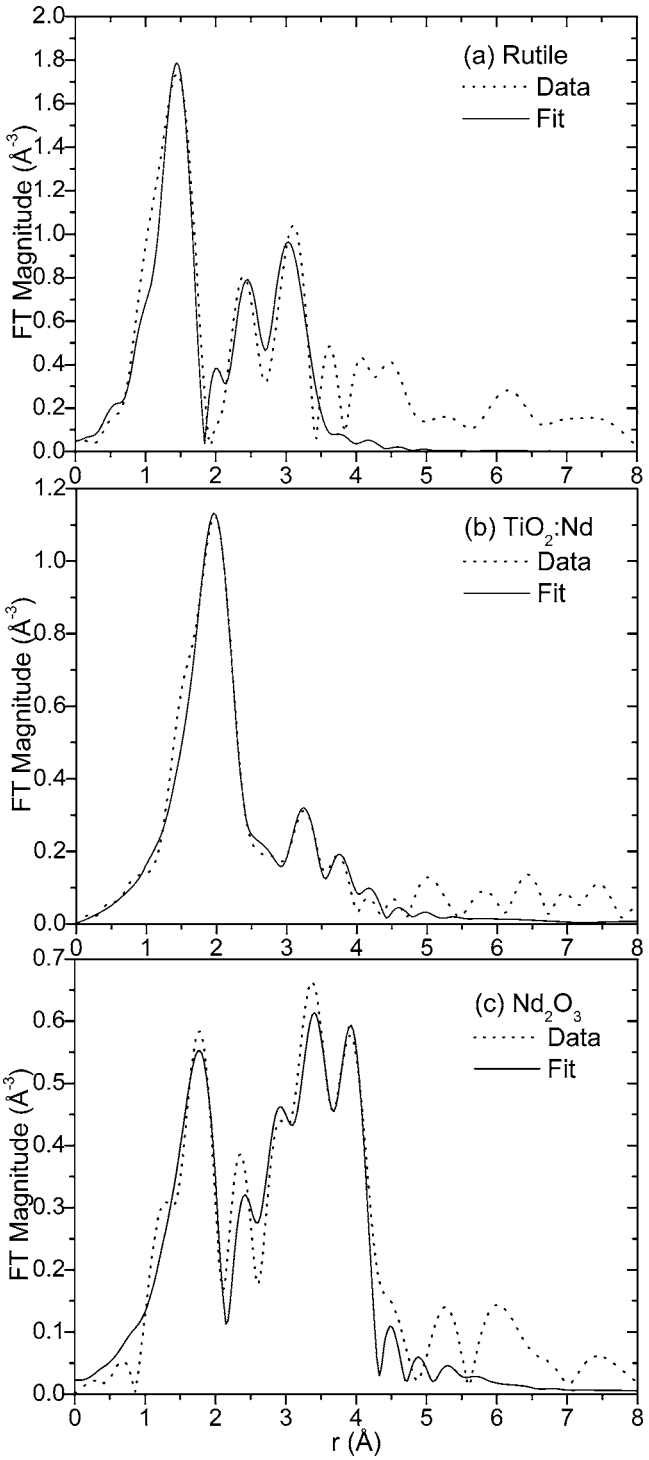


FIG. 5. The Fourier transform magnitudes of EXAFS spectra of $k^2$-weighted $\chi(k)$ data and FEFF6 fits for (a) Ti K-edge for pure rutile $TiO_2$; (b) Nd $L_3$-edge for 1 % of Nd doped $TiO_2$; and (c) Nd $L_3$-edge for $Nd_2O_3$.

The local structure distortion can be revealed in both angular distortion and length distortion of chemical bonds. In anatase, two apical and four equatorial oxygen atoms in the $TiO_6$ octahedron primitive cell form the Ti first O shell (O1) with a local symmetry of $D_{2d}$, whereas in rutile, the local symmetry of Ti-O bonds changes to $D_{2h}$.[30] After the incor-

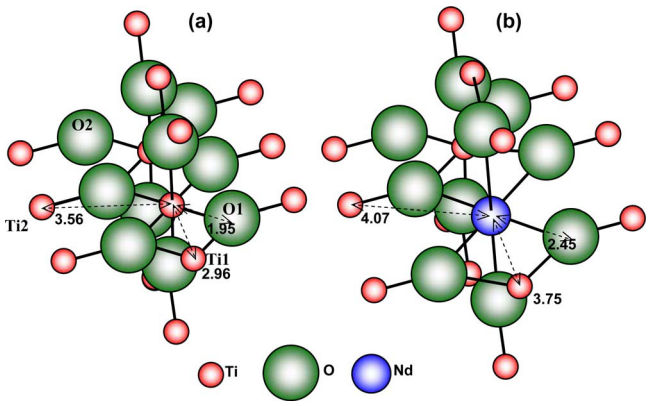


FIG. 6. (Color online) Schematics of (a) rutile structure and (b) rutile like Nd local structure in $TiO_2$ nanoparticles.

poration of Nd, the local structure changes to rutile like formation. Namely, with the Nd ions in the Ti positions, the angle of two equatorial Ti-O bonds (O-Ti-O) increases whereas the angle of one equatorial and one apical Ti-O bond (Ti-O-Ti) decreases. Eventually, the structure is in resemblance to the rutile $TiO_6$ configuration (Fig. 6(b)). Moreover, the change of metal-oxygen and metal-metal bond lengths is also evident (Table I). The measured Ti-O1 and Ti-Ti1 distances ($r$) from Ti to the first O shell and the first Ti shell are 1.95(1) Å and 2.96(2) Å, respectively. However, the large difference from these distances is found in Nd doped samples. For example, the Nd-O1 and Nd-Ti1 lengths in 1 % of Nd doped $TiO_2$ are 2.48(1) Å and 3.75(6) Å, respectively. Very similar results were obtained for 1.5 % of Nd doped $TiO_2$. There is about 0.5 Å length expansion from Ti-O1 to Nd-O1 as well as Ti-Ti2 to Nd-Ti2. In addition, the elongation of the Nd-Ti1 bond length relative to Ti-Ti1 reaches 0.8 Å.

### D. Substitutional $Nd^{3+}$ ions in $TiO_2$ lattice

The change of $TiO_2$ lattice constants and Nd dopant local structure strongly indicates that $Nd^{3+}$ ions have substituted the $Ti^{4+}$ ions. The large difference of ionic radius (~0.4 Å) between $Nd^{3+}$ and $Ti^{4+}$ causes local lattice expansion and the concomitant local strain field at the Nd dopant sites. In addition, the different electronic structure of $Nd^{3+}$ and $Ti^{4+}$ can cause a variation of electronic interactions at the atomic level and further induce the lattice distortions. The electronic effect induced lattice distortion has also been observed in the As doped single crystal Si system.[33] Besides the crystal lattice distortions, the electronic structure and band gap change of doped $TiO_2$ agrees well with the existence of substitutional $Nd^{3+}$ ions.[21]

The substitutional $Nd^{3+}$ is useful to enhance certain properties of $TiO_2$ nanoparticles. For instance, to neutralize the electric charge in $TiO_2$, the substitutional $Nd^{3+}$ ions form Nd-O bonds by introducing possible oxygen vacancies into their vicinity. The empirical composition relation in doped samples can also be formulated as $Nd_xTi_{1-x}O_{2-0.5x}$. The oxygen vacancies have capability to trap photo-excited electrons to increase the lifetime of the holes. Therefore, substitutional

TABLE I. Comparison of Ti-NN and Nd-NN distances in the $TiO_2$ structure for $TiO_2$ and Nd:$TiO_2$ (1% and 1.5% of Nd), respectively. Ti-O2 contributions are not included in TiO2 analysis, since they interfere in the same distance range with Ti-Ti2, as described in the text. Such degeneracy is lifted in the case of Nd:$TiO_2$ EXAFS data.

| NN | N | R (Å) | | |
|---|---|---|---|---|
| | | $TiO_2$ | 1% Nd | 1.5% Nd |
| O1 | 6 | 1.95(1) | 2.48(1) | 2.45(1) |
| Ti1 | 2 | 2.96(2) | 3.75(6) | 3.75(7) |
| Ti2 | 8 | 3.56(3) | 4.07(3) | 4.06(4) |
| O2 | 8 | — | 4.20(4) | 4.18(5) |

doping of $Nd^{3+}$ provides several advantages. For example, it can greatly enhance the photoreactivity of $TiO_2$ nanoparticles not only by realizing visible light absorption but also by achieving high efficient electron/hole separation. The visible light absorption is achieved because the substitutional $Nd^{3+}$ ions introduce electronic states on the bottom of the $TiO_2$ conduction band edge and form a new highest unoccupied molecular orbital to narrow the band gap. The effective charge carrier separation becomes possible due to the strong trapping effect in the lattice induced by the substitutional dopant. We have already experimentally and theoretically confirmed these possibilities.[21]

## IV. CONCLUSION

We have studied the Nd dopant location and lattice structure distortion in the anatase $TiO_2$ nanoparticles synthesized by MOCVD. Nd was determined to have a trivalent chemical state by XPS. Average structural distortion and local structural change in the doped $TiO_2$ nanoparticles were detected by XRD and EXAFS techniques, respectively. The average lattice constant is enlarged along the $c$-axis with a maximum value of 0.15 Å for 1.5 % Nd doped sample. The local structure of Nd is similar to the rutile configuration. The lengths of Nd-O1 and Nd-Ti2 bonds in doped samples have a 0.5 Å increase and the increase of Nd-Ti1 length reaches 0.8 Å compared with Ti associated bonds in a pure $TiO_2$ structure. All these results strongly support that $Nd^{3+}$ ions are situated at the substitutional locations and cause lattice distortions in the $TiO_2$ nanoparticles.

## ACKNOWLEDGMENTS

The authors would like to thank NSF-NIRT (Grant No. DMR-0210284) and the U.S. DOE (Grant No. DE-FG02-03ER15477) for the funding of this project, the U.S. DOE (Grant No. DE-AC02-98CH10886) for the research at the National Synchrotron Light Source, Brookhaven National Laboratory, and the U.S. DOE (Grant No. W-31-109-ENG-38) for the research at the Advanced Photon Source, Argonne National Laboratory.

*Corresponding author. Electronic address: ismat@udel.edu

[1] S. U. M. Khan, M. Al-Shahry, and W. B. Ingler, Science **297**, 2243 (2002).
[2] S. Guha, K. Ghosh, J. G. Keeth, S. B. Ogale, S. R. Shinde, J. R. Simpson, H. D. Drew, and T. Venkatesan, Appl. Phys. Lett. **83**, 3296 (2003).
[3] H. M. Weng, X. P. Yang, J. M. Dong, H. Mizuseki, M. Kawasaki, and Y. Kawazoe, Phys. Rev. B **69**, 125219 (2004).
[4] Y. Matsumoto, M. Murakami, T. Shono, T. Hasegawa, T. Fukumura, M. Kawasaki, P. Ahmet, T. Chikyow, S. Koshihara, H. Koinuma, Science **291**, 854 (2001).
[5] C. Di Valentin, G. Pacchioni, and A. Selloni, Phys. Rev. B **70**, 085116 (2004).
[6] R. F. Howe, Dev. Chem. Eng. Miner. Process. **6**, 55 (1998).
[7] M. A. Barakat, G. Hayes, and S. I. Shah, J. Nanosci. Nanotechnol. **10**, 1 (2005).
[8] E. Borgarello, J. Kiwi, M. Gräetzel, E. Pelizzetti, and M. Visca, J. Am. Chem. Soc. **104**, 2996 (1982).
[9] K. Wilke and H. D. Breuer, J. Photochem. Photobiol., A **121**, 49 (1999).
[10] W. Mu, J. M. Herrmann, and P. Pichat, Catal. Lett. **3**, 73 (1989).
[11] M. Takeuchi, H. Yamashita, M. Matsuoka, M. Anpo, T. Hirao, N. Itoh and N. Iwamoto, Catal. Lett. **67**, 135 (2000).
[12] M. I. Litter and J. A. Navío, J. Photochem. Photobiol., A **98**, 171 (1996).
[13] Y. Ma, X. T. Zhang, Z. S. Guan, Y. A. Cao, and J. N. Yao, J. Mater. Res. **16**, 2928 (2001).
[14] S. M. Karvinen, Ind. Eng. Chem. Res. **42**, 1035 (2003).
[15] G. N. Greaves, A. J. Dent, B. R. Dobson, S. Kalbitzer, S. Pizzini, and G. Muller, Phys. Rev. B **45**, 6517 (1992).
[16] S. W. Wang, A. Y. Borisevich, S. N. Rashkeev, M. V. Glazoff, K. Sohlberg, S. J. Pennycook, and S. T. Pantelides, Nat. Mater. **3**, 143 (2004).
[17] B. D. Padalia, S. J. Gurman, P. K. Mehta and Om. Prakash, J. Phys.: Condens. Matter **4**, 6865 (1992).
[18] A. I. Frenkel, D. M. Pease, J. Giniewicz, E. A. Stern, D. L. Brewe, M. Daniel, and J. Budnick, Phys. Rev. B **70**, 014106 (2004).
[19] G. P. Diakun, L. Fairall, and A. Klug, Nature **324**, 698 (1986).
[20] P. M. Peters and S. N. HoudeWalter, Appl. Phys. Lett. **70**, 541 (1997).
[21] W. Li, Y. Wang, H. Lin, S. I. Shah, C. P. Huang, D. J. Doren, S. A. Rykov, J. G. Chen, and M. A. Barteau, Appl. Phys. Lett. **83**, 4143 (2003).
[22] W. Li, S. I. Shah, M. Sung, and C. P. Huang, J. Vac. Sci. Technol. B **20**, 2303 (2002).
[23] C. D. Wagner, W. M. Riggs, L. E. Davis, and J. F. Moulder, *Handbook of X ray Photoelectron Spectroscopy*, edited by G. E. Muilenberg (Perkin-Elmer Corp., Maryland, 1979).
[24] Y. Uwamino, T. Ishizuka, and H. Yamatera, J. Electron Spectrosc. Relat. Phenom. **34**, 67 (1984).
[25] D. D. Sarma and C. N. R. Rao, J. Electron Spectrosc. Relat. Phenom. **20**, 25 (1980).
[26] R. D. Shannon, Acta Crystallogr. **32**, 751 (1976).
[27] M. Newville, J. Synchrotron Radiat. **8**, 322 (2001).
[28] M. Newville, P. Livins, Y. Yacoby, J. J. Rehr, and E. A. Stern, Phys. Rev. B **47**, 14126 (1993).
[29] S. I. Zabinsky, J. J. Rehr, A. Ankudinov, R. C. Albers, and M. J. Eller, Phys. Rev. B **52**, 2995 (1995).
[30] A. Fahmi, C. Minot, B. Silvi, and S. Causa, Phys. Rev. B **47**, 11717 (1993).
[31] S.-D. Mo and W. Y. Ching, Phys. Rev. B **51**, 13023 (1995).
[32] M. Faucher, J. Dexpert-Ghys, and P. Caro, Phys. Rev. B **21**, 3689 (1980).
[33] A. Erbil, W. Weber, G. S. Cargill, III, and R. F. Boehme, Phys. Rev. B **34**, 1392 (1986).